

Causes of simulated long-term changes in phytoplankton biomass in the Baltic Proper: A wavelet analysis

Jenny Hieronymus¹, Kari Eilola¹, Magnus Hieronymus¹, H. E. Markus Meier^{2,1}, Sofia Saraiva¹, and Bengt Karlson¹

¹Research and Development Department, Swedish Meteorological and Hydrological Institute, Norrköping, Sweden

²Department of Physical Oceanography and Instrumentation, Leibniz Institute for Baltic Sea Research Warnemünde, Rostock, Germany.

Correspondence to: Jenny Hieronymus (jenny.hieronymus@gmail.com)

1 **Abstract.** The co-variation of key variables with simulated phytoplankton biomass in the Baltic proper has been exam-
2 ined using wavelet analysis and results of a long-term simulation for 1850-2008 with a high-resolution, coupled physical-
3 biogeochemical circulation model for the Baltic Sea. By focusing on inter-annual variations it is possible to track effects acting
4 on decadal time scales such as temperature increase due to climate change as well as changes in nutrient input. The strongest
5 inter-annual coherence indicates that variations in phytoplankton biomass are determined by changes in concentrations of the
6 limiting nutrient. However, after 1950 high nutrient concentrations created a less nutrient limited regime and the coherence was
7 reduced. Furthermore, the inter-annual coherence of mixed layer nitrate with riverine input of nitrate is much larger than the
8 coherence between mixed layer phosphate and phosphate loads. This indicates a greater relative importance of the vertical flux
9 of phosphate from the deep layer into the mixed layer. In addition, shifts in nutrient patterns give rise to changes in phytoplank-
10 ton nutrient limitation. The modelled pattern shifts from purely phosphate limited to a seasonally varying regime. The results
11 further indicate some effect of inter-annual temperature increase on cyanobacteria and flagellates. Changes in mixed layer
12 depth affect mainly diatoms due to a high sinking velocity while inter-annual coherence between irradiance and phytoplankton
13 is not found.

14 1 Introduction

15 The Baltic Sea is a semi-enclosed brackish water body separated from the North Sea and Kattegat through the Danish Straits.
16 It stretches from about 54° to 66° N and the limited water exchange with the ocean in the south gives rise to a large meridional
17 salinity gradient. The circulation is estuarine with a salty deep-water inflow from the ocean and a fresher surface outflow. The
18 Baltic Sea comprises a number of sub-basins connected by sills further restricting the circulation.

19 The limited water exchange and the long residence time of water have consequences for the biology and the biogeochemistry.
20 The Baltic Sea is naturally prone to eutrophication and organic matter degradation leads to low deep water oxygen concentra-
21 tions in between deep water renewal events. In turn, this leads to complex nutrient cycling with different processes acting in
22 oxygenized vs low oxygen environments.

23 The Baltic Sea has experienced extensive anthropogenic pressure over the last century. After 1950, intensive use of agricul-
24 tural fertilizer greatly enhanced the nutrient loads. This led to an expansion of hypoxic bottoms (Carstensen et al., 2014), in
25 turn affecting the cycling of nutrients through the system. Anoxic sediments have lower phosphorus retention capacity resulting
26 in increased deep water phosphate concentrations. Thereby, the flux of phosphate to the surface intensified even though the
27 external loads decreased after 1980 in response to improved sewage treatment. Furthermore, as the anoxic area increased, the
28 area of interface between oxic and anoxic zones where denitrification occurs also increased. This resulted in a loss of nitrogen.
29 Vahtera et al. (2007) described these processes as generating a “vicious circle” where decreased DIN concentrations together
30 with increased phosphate enhanced the relative importance of nitrogen fixation by cyanobacteria.

31 The importance of this coupling between oxygen and nutrients have been examined in models. Gustafsson et al. (2012)
32 confirmed, using the model BALTSEM, that internal nutrient recycling has increased due to the reduced phosphate retention
33 capacity, resulting in a self sustained eutrophication where enhanced sedimentary outflux of nutrients together with increased
34 nitrogen fixation outweigh external load reductions.

35 Satellite monitoring has made it possible to observe changes in several physical and ecological surface variables during the
36 past three decades. Significant changes in seasonality have been observed, such as an earlier start of the phytoplankton growth
37 season and timing of chlorophyll maxima (Kahru et al., 2016).

38 Shifts in nutrient composition and deep water properties remain difficult to evaluate using observations. Even though the
39 Baltic Sea has a dense observational record from ships, stations and satellites, the longest nutrient records comprise station
40 data from the early 1970 (HELCOM, 2012). For longer time periods the use of a model is required.

41 In this paper we construct a thorough analysis of the co-variation of phytoplankton biomass with key variables that have
42 been affected by anthropogenic change over the 20th century. Using the biogeochemical model SCOB1 (Eilola et al., 2009;
43 Almroth-Rosell et al., 2011) coupled to the 3d circulation model RCO (Meier et al., 2003) we scrutinize the effect of nutrient
44 loads, nutrient concentration, temperature, irradiance and mixed layer depth on the modelled phytoplankton community.

45 The gap-free dataset provided by the model allows us to decompose the variables in time-frequency space using the wavelet
46 transform. Two variables may than be compared using wavelet coherence (e.g., Torrence and Compo, 1998; Grinsted et al.,
47 2004).

48 We have chosen to use a model run spanning the period 1850 to 2009. Thereby, we capture conditions relatively unaf-
49 fected by anthropogenic forcing as well as current conditions of eutrophication and climate change. Furthermore, we limit our
50 investigation to the Baltic Proper so as to capture relatively homogenous conditions with regards to the biology.

51 **2 Methods**

52 **2.1 Model**

53 We have used a run from the model RCO-SCOB1 spanning 1850-2009. RCO (Rossby Centre Ocean model) is a three-
54 dimensional regional ocean circulation model (Meier et al., 2003). It is a z-coordinate model with a free surface and an

55 open boundary in the northern Kattegat. The version used here has a horizontal resolution of 2nm with 83 depth levels at 3m
56 intervals.

57 The biogeochemical interactions are solved by the Swedish Coastal and Ocean Biogeochemical model (SCOBI) (Eilola
58 et al., 2009; Almroth-Rosell et al., 2011). The model contains the nutrients phosphate, nitrate and ammonia as well as the
59 plankton functional types representing diatoms, flagellates and others (will be referred to as flagellates from here on) and
60 cyanobacteria. Furthermore, the model contains nitrogen and phosphorus in one active homogenous benthic layer.

61 The model equations can be found in Eilola et al. (2009). Since we are exploring the effect of different variables on the
62 growth of phytoplankton we will, for clarity, repeat some of them here.

63 The phytoplankton biomass is described in terms of chlorophyll and with a constant C:Chl ratio. The model thus does not
64 take into account seasonal changes in C:Chl as was found by Jakobsen and Markager (2016).

65 The net growth of phytoplankton (PHY) is described by the following expression,

$$66 \text{GROWTH}_{\text{PHY}} = \text{ANOX} \cdot \text{LTLIM} \cdot \text{NUTLIM}_{\text{PHY}} \cdot \text{GMAX}_{\text{PHY}} \cdot \text{PHY}. \quad (1)$$

67 Subscript PHY indicates the plankton funktional type (diatoms, flagellates or cyanobacteria). ANOX is a logarithmic expres-
68 sion that approaches zero as the oxygen concentration becomes small.

69 LTLIM expresses the phytoplankton light limitation and NUTLIM describes the nutrient limitation. Nutrient limitation
70 follows Michaelis-Menten kinetics where constant Redfield ratios are assumed in nutrient uptake. NUTLIM is further described
71 in Sects. 2.1.1 and 2.1.2. GMAX is temperature dependent and describes the maximum phytoplankton growth rate.

72 Diatoms and flagellates have different halfsaturation constants, maximum growth rate, temperature dependence and sinking
73 rate. Flagellates are more sensitive to changes in temperature than diatoms. Furthermore, the sinking rate of diatoms is five
74 times larger than that for flagellates.

75 The difference between cyanobacteria and the other phytoplankton is more pronounced. Cyanobacteria can grow either
76 according to Eq. (1) or using nitrogen fixation. The rate of nitrogen fixation is a function of phosphate concentration, N:P
77 ratio and temperature. Both nitrogen fixation and GROWTH of cyanobacteria is zero if the salinity is above 10. Furthermore,
78 cyanobacteria is the most temperature sensitive of the phytoplankton groups and no sinking is assumed.

79 Other processes important for our results involves chemical reactions occurring in the water column or in the sediment.
80 Denitrification occurs both in the water column and the benthic layer and constitutes a sink for nitrate in case of anoxia.
81 Nitrification transforms ammonium into nitrate as long as oxygen is present. Phosphorus is adsorbed to the sediment and
82 the benthic release capacity of phosphate is a function of the oxygen concentration. The phosphorus release capacity is also
83 dependent on salinity whereby higher salinity leads to lower retention of phosphate in the benthic layer.

84 **2.1.1 Nutrient limitation**

85 Estimating nutrient limitation in nature is difficult. Usually this is done, either by comparing nutrient ratios to Redfield in, e.g.,
86 the surface water or external supply or through nutrient enrichment experiments (Granéli et al., 1990).

87 The implementation of nutrient limitation most commonly used is that the primary production is directly limited by the
 88 nutrient concentration in the ambient water and that the internal nutrient ratios in the phytoplankton are constant, i.e., in accor-
 89 dance with a Redfield-Monod model (Redfield, 1958). However, cell-quota type models (Droop, 1973) are being increasingly
 90 implemented and the use of constant internal nutrient ratios are becoming more and more questioned (Flynn, 2010; Fransner
 91 et al., 2018).

92 In our model, nutrient limitation is expressed assuming constant Redfield ratios and phytoplankton growth is limited by
 93 either nitrogen or phosphate. The degree of nutrient limitation is described by

$$94 \text{NUTLIM}_{\text{PHY}} = \min(\text{NLIM}_{\text{PHY}}, \text{PLIM}_{\text{PHY}}) \quad (2)$$

95 where NLIM_{PHY} and PLIM_{PHY} are the nitrogen and phosphate limitation respectively. NLIM_{PHY} is defined as

$$96 \text{NLIM}_{\text{PHY}} = \begin{cases} \text{NO}_3\text{LIM}_{\text{PHY}} + \text{NH}_4\text{LIM}_{\text{PHY}}, & \text{if } \text{NO}_3\text{LIM}_{\text{PHY}} + \text{NH}_4\text{LIM}_{\text{PHY}} < 1 \\ 1, & \text{otherwise,} \end{cases} \quad (3)$$

97 where

$$98 \text{NO}_3\text{LIM} = \frac{\text{NO}_3}{\text{KNO}_3\text{PHY} + \text{NO}_3} \cdot \exp(-\phi_{\text{PHY}} \cdot \text{NH}_4), \quad (4)$$

$$99 \text{NH}_4\text{LIM} = \frac{\text{NH}_4}{\text{KNH}_4\text{PHY} + \text{NH}_4}, \quad (5)$$

100 where NO_3 and NH_4 are the concentrations of nitrate and ammonium and KNO_3PHY and KNH_4PHY are the halfsaturation
 101 constants for nitrate and ammonium respectively. The exponent in (4) accounts for inhibition of nitrate uptake (e.g., Dortch,
 102 1990; Parker, 1993).

103 PLIM_{PHY} is equal to PO_4LIM which is modelled as

$$104 \text{PO}_4\text{LIM} = \frac{\text{PO}_4}{\text{KPO}_4\text{PHY} + \text{PO}_4}. \quad (6)$$

105 Nutrient limitation, NUTLIM , is thus described by a number between 0 and 1 where 1 is no limitation. The constant
 106 KPO_4PHY is the half saturation constants for phosphate and the constant ϕ_{PHY} in Eq. (4) determines the strength of am-
 107 monium inhibition of nitrate uptake. Since NUTLIM is calculated as the minimum of NLIM and PLIM , NLIM larger than
 108 PLIM will temporally cause P limitation of phytoplankton growth rate. Hence, a different formulation e.g. of NLIM might
 109 change a models sensitivity to the limiting nutrient. Its impact on system nutrient dynamics on longer time scales is, however,
 110 difficult to judge because e.g. nitrogen fixation and denitrification potentially also may be influenced. Further experiments on
 111 this issue are out of the scope of the present paper and left for future studies.

112 NUTLIM for our model run has been calculated offline from the monthly means according to Eq. (2).

113 **2.1.2 Effect of physical parameters**

114 Changes in cloud-cover affect the incoming solar radiation and thereby phytoplankton growth. The effect of light is given by
115 the LTLIM term of Eq. (1) which accounts for photo-inhibition.

116 The mixed layer depth has been defined as the depth where a density difference of 0.125 kg m^{-3} from the surface occurs in
117 accordance with what was previously done by e.g., Eilola et al. (2013). The density was calculated from modelled temperature
118 and salinity using the algorithms from Jackett et al. (2006).

119 **2.2 Study area**

120 The Baltic Sea contains several different sub-basins with different characteristics in salinity and nutrient loads. In this study
121 we focus on the Baltic proper as defined in Fig. 1. In order to reduce heterogeneity we exclude areas shallower than 20m and
122 put our focus away from the coasts.

123 We have chosen to use a basin averaged approach in order to remove local variability and gain a better understanding of
124 the system. All variables have thus been horizontally averaged over the study area. Furthermore, we have also averaged all
125 variables over the mixed layer and from the mixed layer down to a depth of 150m.

126 **2.3 Forcing**

127 The study use reconstructed (1850-2008) atmospheric, hydrological and nutrient load forcing and daily sea levels at the lateral
128 boundary as described by Gustafsson et al. (2012) and Meier et al. (2012). Monthly mean river flows were merged from
129 reconstructions by Hansson et al. (2011) and Meier and Kauker (2003) and hydrological model data from Graham (1999),
130 respectively. For further details about the physical model setup used in the present study the reader is referred to Meier et al.
131 (2017) and references therein.

132 The nutrient input from rivers and point sources were (1970-2006) compiled from the Baltic Environmental and HELCOM
133 databases (Savchuk et al., 2012). Estimates of pre-industrial loads for 1900 were based on data from Savchuk et al. (2008).
134 The nutrient loads were linearly interpolated between selected reference years in the period between 1900 and 1970. Similarly,
135 atmospheric loads were estimated (Ruoho-Airola et al., 2012). Nutrient loads contain both organic and inorganic phosphorus
136 and nitrogen, respectively. For riverine organic phosphorus and nitrogen loads bioavailable fractions of 100 and 30% are
137 assumed, respectively.

138 The upper panel of Fig. 2 shows the input of Dissolved Inorganic Phosphorus (DIP) and Dissolved Inorganic Nitrogen (DIN)
139 to the Baltic Proper as defined in Fig. 1. The lower panel shows the corresponding simulated mixed layer concentrations. The
140 loads have been calculated from the runoff and annual mean nutrient concentrations (Eilola et al., 2011). Thus the seasonal
141 cycle in river loads is determined by the runoff. After a spin-up simulation for 1850-1902 utilizing the reconstructed forcing as
142 described above, the calculated physical and biogeochemical variables at the end of the spin-up simulation were used as initial
143 condition for 1850. We have used riverine DIN and DIP loads for our analysis. The use of total bioavailable nutrient loads
144 instead does not change the results.

145 The open boundary conditions in the northern Kattegat were based on climatological (1980-2000) seasonal mean nutrient
146 concentrations (Eilola et al., 2009). Similar to Gustafsson et al. (2012) a linear decrease of nutrient concentrations back in
147 time was added assuming that climatological concentrations in 1900 amounted to 85% of present day concentrations (Savchuk
148 et al., 2008). The bioavailable fraction of organic phosphorus at the boundary was assumed to be 100% in accordance with
149 the organic phosphorus supply from land runoff. Organic nitrogen was implicitly added because of the Redfield ratio of model
150 detritus (Eilola et al., 2009).

151 **2.4 Evaluation**

152 The specific model setup used here have been shown to agree well with observations for salinity, temperature and nutrients
153 (Meier et al., in press; Eilola et al., 2014). The different phytoplankton functional types have not been previously validated
154 against observations.

155 Fig. 3 shows the different simulated phytoplankton together with observations at the monitoring station BY15 (see Fig.1).
156 Monthly means and standard deviations are shown in Fig. 4. The observational dataset has been recalculated from biovolumes
157 to carbon units in accordance with Menden-Deuer and Lessard (2000). The simulated values have been recalculated from units
158 of chlorophyll to carbon through a fixed C:Chl ratio of 50 which is in the mid range of the salinity dependent span found by
159 Rakko and Seppälä (2014).

160 The time-series display significant interannual variability in both model and observations. This variability is also visible
161 as large standard deviations in the modelled and observed monthly means in Fig. 4. Fig. 4 also shows an autumn diatom
162 bloom in the observations while the model generates an autumn flagellate bloom. The simulated cyanobacteria bloom occurs
163 approximately two months too late compared to observations. It is also notable that the cyanobacteria displays strong blooms
164 the first four years in both model and observations but that the observations show diminished blooms during the rest of the
165 period where the simulated biomass is still high.

166 Differences in absolute numbers between observations and simulated values can result from the choice of the fixed Chl:C ra-
167 tio. Furthermore, the estimated carbon content from observations are potentially affected by patchiness during in-situ sampling
168 and uncertainties related to the calculation of biovolumes and transformation to carbon units.

169 **2.5 The wavelet transform and wavelet coherence**

170 Several studies have covered the wavelet transform and its application in depth (e.g., Lau and Weng, 1995; Torrence and
171 Compo, 1998; Carey et al., 2016; Grinsted et al., 2004) and here we provide a description of the method.

172 The continuous wavelet transform provides a method to decompose a signal into time-frequency space. In that it is similar
173 to the windowed Fourier transform where the signal is decomposed within a fixed time-frequency window which is then slid
174 along the time-series. However, the fixed width of the window leads to an underestimation of low frequencies. In comparison,
175 the wavelet transform utilizes wavelets with a variable time-frequency window. Wavelets can have many different shapes and
176 the choice is not arbitrary. We have chosen the commonly used Morlet wavelet providing good time and frequency localization
177 (Grinsted et al., 2004).

178 In time-series with clear periodic patterns affected by environmental variables such as population dynamics and ecology the
179 benefits of this approach are significant (Cazelles et al., 2008). In recent years, several studies have highlighted the usefulness
180 of wavelet analyses in plankton research (Winder and Cloern, 2010; Carey et al., 2016). The focus has been the increased
181 availability of long observational data sets making it possible to use the wavelet transform to investigate changes in seasonality.
182 Carey et al. (2016) discussed how the wavelet transform can be used to track interannual changes in phytoplankton biomass and
183 applied it to a 16-year time series of phytoplankton in Lake Mendota, USA. In doing so they were able to identify periods when
184 the annual periodicity was less pronounced. They discussed the benefit of this technique in scrutinizing changes to the seasonal
185 succession due to changes in external drivers. Winder and Cloern (2010) applied the technique to time-series of chlorophyll-a
186 from marine and freshwater localities and discussed the annual and seasonal periodicities.

187 Wavelet coherence further expands the usefulness of the wavelet approach by allowing calculation of the time resolved
188 coherence between two time-series (Grinsted et al., 2004; Cazelles et al., 2008). In this way, it is possible to identify transient
189 periods of correlation over different periodicities. The result is given as coherency as a function of time and period as well as a
190 phase lag between the two time-series.

191 The problem with the wavelet transform is that it requires a dataset without gaps. The time-series also needs to be suffi-
192 ciently long. This impedes the wavelet analysis on longer time scales such as the time scale of changing climate because long
193 observational datasets are lacking. Hence, for our purpose only a model based approach is feasible.

194 Schimanke and Meier (2016) used wavelet coherency on a multi-centennial model run to evaluate the correlation of different
195 forcing variables with the Baltic Sea salinity. Here we analyze the coherence between modelled phytoplankton biomass and a
196 few key modelled and forcing variables.

197 For all wavelet calculations we use the Matlab wavelet package described in Grinsted et al. (2004), which is freely available
198 at <http://www.glaciology.net/wavelet-coherence>.

199 **3 Results and discussion**

200 We will begin in Sect. 3.1 by presenting the model results on phytoplankton biomass. In Section 3.2 we will present the
201 nutrients and their coherence with the phytoplankton biomass. Coherence between riverine loads and mixed layer nutrients
202 will be discussed in Sect. 3.3. Section 3.4 examines the coherence of phytoplankton with temperature and irradiance. Finally,
203 the coherence between mixed layer depth and phytoplankton biomass is considered in Sect. 3.5. All results shown are monthly
204 means.

205 **3.1 Phytoplankton biomass**

206 Fig. 5 shows the time-series of phytoplankton biomass (a) together with the corresponding wavelet spectrum (b).

207 The wavelet power (variance) of the decomposed signal (in color) is displayed as a function of time (x-axis) and period
208 (y-axis). The black curves in Fig. 5(b) show the 95% confidence level relative to red noise.

209 Averaging over time generates the global power spectrum displayed in Fig. 5 (c). The wavelet spectrum clearly reveals two
210 main periodicities - the annual and the semi-annual representing the spring and autumn blooms. It is also clearly visible that
211 the power on both periodicities increases markedly after 1950.

212 Kahru et al. (2016) found a shift in chlorophyll maxima from the diatom dominated spring bloom to the cyanobacteria sum-
213 mer bloom. A similar pattern emerges from our model run as can be seen in Fig. 6. The figure shows the month of maximum
214 biomass of the different phytoplankton species as well as the month of maximum chlorophyll (diatoms+flagellates+cyanobacteria).
215 After 1998 the results display five years where the month of maximum chlorophyll corresponds to the month of maximum
216 cyanobacteria biomass in August or September.

217 **3.2 Nutrients and nutrient limitation**

218 Increased nutrient loads have caused a strengthening of the primary production and thereby also the deep water respiration,
219 resulting in a 10-fold increase in hypoxic area since the beginning of the 20th century (Carstensen et al., 2014). This has led
220 to changing nutrient patterns as have been discussed by (e.g., Conley et al., 2002; Savchuk, 2010, 2018; Vahtera et al., 2007).
221 Anoxia causes sedimentary phosphate release. A clear relationship between hypoxia and total basin averaged phosphate was
222 first shown by Conley et al. (2002) (and later expanded by Savchuk (2010)) on observational data from the Baltic Proper.

223 The effect of hypoxia on DIN is less straight forward. Expanding hypoxia increases the boundary area between anoxic and
224 oxic water where denitrification occurs resulting in a loss of nitrate. Furthermore, hypoxia causes a reduction in nitrification
225 leading to a further reduction in nitrate. Vahtera et al. (2007) found a negative relationship between basin averaged DIN and
226 hypoxic area in observations from the Baltic Sea.

227 The changing nutrient patterns for our model run are shown in Fig. 7. In conjunction with the increased anoxic volume
228 we find a clear increase in ammonium and a decrease in nitrate. This is due to a decrease in nitrification and an increase
229 in denitrification. The phosphate concentration increases from the mid 20th century through the rest of the model run as a
230 combined effect of the accumulated terrestrial inputs and hypoxic sedimentary release.

231 The effect of nutrients on the primary production is in the model controlled by the term NUTLIM, or degree of nutrient
232 limitation, in Eq. (1). NUTLIM can be viewed as a measure of the nutrient composition that linearly affects the phytoplankton
233 growth in the model. We examine this term in as well as below the mixed layer as changes in the concentration of nutrients in
234 the deep water will affect also nutrient concentrations in the mixed layer.

235 The evolutions of NUTLIM in the mixed layer and deep water for diatoms and flagellates are shown in Fig. 8. There is a
236 clear increase over the 20th century and a shift towards less limited conditions (NUTLIM approaching 1).

237 Nitrogen has been shown to most often limit the growth in the Baltic Proper, while phosphate is limiting in the northern
238 basins (Granéli et al., 1990; Tamminen and Andersen, 2007). In pre-industrial conditions, N/P ratios indicate a lesser degree
239 of nitrogen limitation and a higher degree of phosphate limitation for the central Baltic Sea (Schernewski and Neumann, 2004;
240 Savchuk et al., 2008; Gustafsson et al., 2012). The mixed layer limitation pattern in our model run as calculated with N/P
241 ratios is shown in the lower panel of Fig. 9. Until 1980 the results show a pattern of limitation shifting between nitrogen and

242 phosphate whereafter persistent N limitation develops. This weaker N limitation during the first part of the run is consistent
243 with above mentioned studies of pre-industrial conditions.

244 Using the model's definition of nutrient limitation, our model results, shown in Fig. 9, display phosphate limitation for both
245 diatoms and flagellates for the earlier part of the run. After 1980, a different seasonal pattern appears with phosphate still
246 limiting during winter while nitrogen becomes limiting after the spring bloom. Even though the limitation pattern as calculated
247 with NUTLIM differs from what was found using N/P ratios, the overall pattern of increasing degree of N limitation is evident
248 in NUTLIM as well.

249 The changing nutrient limitation patterns affect phytoplankton growth. We analyse the wavelet coherencies of phytoplankton
250 biomass with mixed layer phosphate and DIN in Figs. 10 and 11.

251 As the strongest nutrient limited group, diatoms show persistent inter-annual coherence with phosphate during the first,
252 consistently phosphate limited part of the run (Fig. 10, see also Fig. 9).

253 Since nitrogen limitation as calculated with NUTLIM mostly occurs after 1980 and after the spring bloom (Fig. 9), and thus
254 only affects the much smaller diatom and flagellate autumn blooms, little coherence between phytoplankton and nitrogen can
255 be observed on inter-annual time-scales (Fig. 11).

256 To scrutinize the shift in deep water nutrient composition and the coherence with phytoplankton, we calculate the wavelet
257 coherence between below mixed layer NUTLIM and the diatom and flagellate biomass. The result is shown in Fig. 12. After
258 1980 the phase arrows within the annual coherence period change direction. For diatoms, the phase shifts from NUTLIM
259 preceding diatoms by three months to diatoms preceding NUTLIM by the same amount. Flagellates display a similar shift.

260 The month of maximum NUTLIM shown in Fig. 13, indicates the month when the nutrient composition is most beneficial
261 for phytoplankton growth. The figure shows a clear shift occurring after 1980. Below the mixed layer, NUTLIM changes its
262 maxima from December and January to July, August and September for both diatoms and flagellates while a slight shift from
263 February to March occurs in mixed layer NUTLIM for diatoms. Mixed layer NUTLIM for flagellates displays no clear shift.
264 The shift in NUTLIM is a result of the increase in phosphate and ammonium occurring in conjunction with the increase in
265 anoxic volume shown in Fig. 7. The change in timing is probably due to reduced sedimentary phosphate retention and reduced
266 nitrification after the spring bloom.

267 **3.3 Nutrient loads**

268 We here analyze how changes in nutrient loads affect changes in the mixed layer nutrient concentrations.

269 The wavelet coherence between mixed layer nutrients and riverine input is shown in Fig. 14. The phosphate loads show little
270 coherence on periodicities longer than one year but DIN displays strong inter-annual coherence. The phase-arrows indicate a
271 phase-lag of about minus 45° on all inter-annual periodicities. For an 8 year period this means that a change in riverine input
272 precedes changes in mixed layer DIN by about 1 yr.

273 To further investigate the lack of inter-annual coherence between riverine phosphate loads and mixed layer phosphate, the
274 wavelet coherence between mixed layer salinity and nutrients are examined and displayed in Fig. 15. Mixed layer salinity is
275 affected by freshwater input from land, water exchange with adjacent basins, precipitation, evaporation and mixing with deeper

276 layers. The coherence spectrum reveals higher coherence between mixed layer salinity and phosphate (top) on interannual
277 periodicities than between salinity and DIN (bottom). The coherence that does exist between salinity and DIN on periodicities
278 longer than one year is antiphase i.e. low salinity here coheres with high DIN concentrations. This indicates that high runoff is
279 connected to high nitrogen loads and high DIN concentrations in the mixed layer. It is also possible that low salinity in the mixed
280 layer indicate periods with deep mixing and better oxygen conditions in and below the halocline (Stigebrandt and Gustafsson,
281 2007). This could reduce the denitrification during these periods and thus result in higher mixed layer DIN concentrations.

282 In contrast, the stronger inter-annual in-phase coherence between salinity and phosphate suggests that the reason for the
283 coherence might be a greater importance of phosphorus release from the sediments that eventually reaches the mixed layer
284 through mixing with deeper layers (cf. Eilola et al., 2014).

285 Riverine nutrient loads show little inter-annual coherence with phytoplankton biomass (not shown) other than on a 16 yr
286 period which probably reflects the overall pattern of simultaneous increase in riverine loads and phytoplankton biomass over
287 the second half of the 20th century.

288 **3.4 Temperature and irradiance**

289 The mixed layer temperature has increased over the 20th century (not shown). To analyze the effect of temperature on the
290 phytoplankton biomass, the wavelet coherence between temperature and phytoplankton have been plotted in Fig. 16. The
291 results suggest that the temperature increase after 1990 might have had an effect on cyanobacteria and flagellates. It is also
292 noticeable that the temperature increase observed between 1900 and 1940 probably had an effect on cyanobacteria. This is also
293 in agreement with the model formulation where cyanobacteria are the most sensitive to temperature followed by flagellates.

294 Light impacts primary production through the term LTLIM in Eq. (1). However, irradiance display very little variation on
295 any other periodicity than the annual as can be observed in a wavelet power spectrum (not shown). Therefore there exists
296 almost no coherence between phytoplankton and irradiance apart from the seasonal signal.

297 **3.5 Mixed layer depth**

298 We calculate the coherence between mixed layer depth and diatoms, flagellates and cyanobacteria in Fig. 17.

299 Apart from the annual cycle there is a strong coherence between mixed layer depth and diatoms, and to some extent flag-
300 ellates, on shorter periodicities as well. That is, the diatom biomass residing in the mixed layer seems to covary quite well
301 on periodicities equal to or shorter than one year. The model value for diatom sinking rate is five times higher than that for
302 flagellates while cyanobacteria is assumed to have no sinking rate. In a shallow mixed layer the diatom biomass decreases
303 faster than in a deep mixed layer because of the large sinking rate. Furthermore, in a deeper mixed layer stronger turbulence
304 counteract the sinking. In the wavelet coherence spectrum we thus see in-phase short term coherence.

305 **4 Conclusions**

306 With a focus on simulated inter-annual variations, the wavelet coherence of the mixed layer phytoplankton biomass with key
307 variables affecting the primary production has been examined for the Baltic Proper.

308 The simulated chlorophyll concentration maximum shifted from spring to late summer at the end of the 20th century in
309 agreement with Kahru et al. (2016).

310 The phytoplankton group most strongly limited by nutrients in the model is diatoms. The connection between primary
311 production and nutrients is reflected in the strong inter-annual coherence between diatoms and phosphate as well as NUTLIM
312 before 1940. After 1940 NUTLIM and the biomass of the individual phytoplankton species have gained such high values that
313 smaller inter-annual variations have relatively little effect on the production. Similarly, flagellates which are less limited by
314 nutrients than diatoms show much smaller inter-annual coherence with phosphate even before 1940. NUTLIM for this group
315 is high enough that small long-term variations do not reflect strongly in the results.

316 Very little inter-annual coherence is observed also between phytoplankton and DIN. Using the models definition of nutrient
317 limitation, the spring bloom is phosphate limited throughout the run except for a few years after 1990 where diatoms are
318 limited by nitrogen. Calculating instead limitation as given by mixed layer N/P ratios generates a pattern in line with previous
319 estimates (Schernewski and Neumann, 2004; Savchuk et al., 2008; Gustafsson et al., 2012).

320 We found strong coherence between riverine input of DIN and mixed layer DIN but not a similar relationship between
321 riverine phosphate input and the corresponding mixed layer concentration. As mixed layer salinity displayed in-phase inter-
322 annual coherence with phosphate and only weak anti-phase coherence with DIN we hypothesise that this is due to a greater
323 importance of the flux of phosphate from lower layers.

324 The mixed layer temperature in the Baltic Proper has increased during the 20th century. We found some response of this
325 mainly from the most temperature sensitive phytoplankton group cyanobacteria during periods of large interannual temperature
326 increases. Flagellates, being more temperature sensitive than diatoms, seems to display a coherence with the temperature
327 increase occurring after 1980.

328 Variations in mixed layer depth affects mainly diatoms as these have a high sinking velocity. In-phase coherence between
329 diatoms and mixed layer depth on periodicities shorter than one year indicates that large seasonal changes in the mixed layer
330 depth significantly affects the mixed layer diatom biomass, while smaller interannual variations are of little consequence.

331 Interannual variations in irradiance are unimportant for phytoplankton biomass.

332 **5 Data availability**

333 The model data on which the results in the present study are based on are stored and available from the Swedish Meteorological
334 and Hydrological Institute. Please send your request to ocean.data@smhi.se.

335 *Acknowledgements.* This work was funded by the Swedish Research Council (VR) within the project “ Reconstruction and projecting Baltic
336 Sea climate variability 1850-2100” (Grant 2012-2117).

337 Funding was also provided by the Swedish Research Council for Environment, Agricultural Sciences and Spatial Planning (FORMAS)
338 within the project “Cyanobacteria life cycles and nitrogen fixation in historical reconstructions and future climate scenarios (1850-2100) of
339 the Baltic Sea” (grant no. 214-2013-1449). The study contributes also to the BONUS BalticAPP (Wellbeing from the Baltic Sea - applications
340 combining natural science and economics) project which has received funding from BONUS, the joint Baltic Sea research and development
341 programme.

342 This research is also part of the BIO-C3 project and has received funding from BONUS, the joint Baltic Sea research and development
343 programme (Art 185), funded jointly from the European Union’s Seventh Programme for research, technological development and demon-
344 stration and from national funding institutions.

345 We thank two anonymous referees for their insightful comments and suggestions that greatly improved the manuscript.

346 References

- 347 Almroth-Rosell, E., Eilola, K., Meier, H. E. M., and Hall, P. O. J.: Transport of fresh and resuspended particulate organic material in the
348 Baltic Sea - a model study, *Journal of Marine Systems*, doi:doi:10.1016/j.jmarsys.2011.02.005, 2011.
- 349 Carey, C. C., Hanson, P. C., Lathrop, R. C., and St. Amand, A. L.: Using wavelet analyses to examine variability in phytoplankton seasonal
350 succession and annual periodicity, *Journal of Plankton Research*, 38, 27–40, doi:10.1093/plankt/fbv116, <http://www.plankt.oxfordjournals.org/lookup/doi/10.1093/plankt/fbv116>, 2016.
- 352 Carstensen, J., Andersen, J. H., Gustafsson, B. G., and Conley, D. J.: Deoxygenation of the Baltic Sea during the last century, *Proceed-*
353 *ings of the National Academy of Sciences*, 111, 5628–5633, doi:10.1073/pnas.1323156111, <http://www.pnas.org/cgi/doi/10.1073/pnas.1323156111>, 2014.
- 355 Cazelles, B., Chavez, M., Berteaux, D., Ménard, F., Vik, J. O., Jenouvrier, S., and Stenseth, N. C.: Wavelet analysis of ecological time series,
356 *Oecologia*, 156, 287–304, doi:10.1007/s00442-008-0993-2, 2008.
- 357 Conley, D. J., Humborg, C., Rahm, L., Savchuk, O. P., and Wulff, F.: Hypoxia in the Baltic Sea and Basin-Scale Changes in Phosphorus
358 Biogeochemistry, *Environ. Sci. Technol.*, 36, 5315–5320, doi:10.1021/es025763w, 2002.
- 359 Dortch, Q.: The interaction between ammonium and nitrate uptake in phytoplankton, *Marine Ecology Progress Series*, 61, 183–201,
360 doi:10.3354/meps061183, 1990.
- 361 Droop, M.: Some thoughts on nutrient limitation in algae, *Journal of Phycology*, 9, 264–272, doi:10.1111/j.1529-8817.1973.tb04092.x, 1973.
- 362 Eilola, K., Meier, H. E. M., and Almroth, E.: On the dynamics of oxygen, phosphorus and cyanobacteria in the Baltic Sea; A model study,
363 *Journal of Marine Systems*, 75, 163–184, doi:10.1016/j.jmarsys.2008.08.009, <http://dx.doi.org/10.1016/j.jmarsys.2008.08.009>, 2009.
- 364 Eilola, K., Gustafsson, B. G., Kuznetsov, I., Meier, H. E. M., Neumann, T., and Savchuk, O. P.: Evaluation of biogeochemical
365 cycles in an ensemble of three state-of-the-art numerical models of the Baltic Sea, *Journal of Marine Systems*, 88, 267–284,
366 doi:10.1016/j.jmarsys.2011.05.004, <http://dx.doi.org/10.1016/j.jmarsys.2011.05.004>, 2011.
- 367 Eilola, K., Mårtensson, S., and Meier, H. E. M.: Modeling the impact of reduced sea ice cover in future climate on the Baltic Sea biogeo-
368 chemistry, *Geophysical Research Letters*, 40, 149–154, doi:10.1029/2012GL054375, 2013.
- 369 Eilola, K., Almroth-Rosell, E., and Meier, H. E. M.: Impact of saltwater inflows on phosphorus cycling and eutrophication in the Baltic Sea:
370 a 3D model study, *Tellus A*, <http://dx.doi.org/10.3402/tellusa.v66.23985>, 2014.
- 371 Flynn, K. J.: Ecological modelling in a sea of variable stoichiometry: Dysfunctionality and the legacy of Redfield and Monod, *Progress in*
372 *Oceanography*, 54, 52–65, doi:10.1016/j.pocean.2009.09.006, <http://dx.doi.org/10.1016/j.pocean.2009.09.006>, 2010.
- 373 Fransner, F., Gustafsson, E., Tedesco, L., Vichi, M., Hordoir, R., Roquet, F., Spilling, K., Kuznetsov, I., Eilola, K., Mörth, C., Humborg,
374 C., and Nycander, J.: Non-Redfieldian Dynamics Explain Seasonal pCO₂ Drawdown in the Gulf of Bothnia, *Journal of Geophysical*
375 *Research: Oceans*, 123, 166–188, doi:10.1002/2017JC013019, <https://agupubs.onlinelibrary.wiley.com/doi/abs/10.1002/2017JC013019>,
376 2018.
- 377 Graham, L. P.: Modeling runoff to the Baltic Sea, *Ambio*, 28, 328–334, 1999.
- 378 Granéli, E., Wallström, K., Larsson, U., Granéli, W., and Elmgren, R.: Nutrient limitation of primary production in the Baltic Sea Area,
379 *Ambio*, 19, 1990.
- 380 Grinsted, a., Moore, J. C., and Jevrejeva, S.: Application of the cross wavelet transform and wavelet coherence to geophysical time series,
381 *Nonlinear Processes in Geophysics*, 11, 561–566, doi:10.5194/npg-11-561-2004, <http://www.nonlin-processes-geophys.net/11/561/2004/>,
382 2004.

383 Gustafsson, B. G., Schenk, F., Blenckner, T., Eilola, K., Meier, H. E. M., Müller-Karulis, B., Neumann, T., Ruoho-Airola, T., Savchuk, O. P.,
384 and Zorita, E.: Reconstructing the development of baltic sea eutrophication 1850-2006, *Ambio*, 41, 534–548, doi:10.1007/s13280-012-
385 0318-x, 2012.

386 Hansson, D., Eriksson, C., Omstedt, A., and Chen, D.: Reconstruction of river runoff to the Baltic Sea, AD 1500-1995, *International Journal*
387 *of Climatology*, 31, 696–703, doi:10.1002/joc.2097, 2011.

388 HELCOM: Approaches and methods for eutrophication target setting in the Baltic Sea region., *Balt. Sea Env. Proc. No. 1*, 2012., 2012.

389 Jackett, D. R., McDougall, T. J., Feistel, R., Wright, D. G., and Griffies, S. M.: Algorithms for density, potential temperature, con-
390 servative temperature, and the freezing temperature of seawater, *Journal of Atmospheric and Oceanic Technology*, 23, 1709–1728,
391 doi:10.1175/JTECH1946.1, 2006.

392 Jakobsen, H. H. and Markager, S.: Carbon-to-chlorophyll ratio for phytoplankton in temperate coastal waters: Seasonal patterns and rela-
393 tionship to nutrients, *Limnol. Oceanogr.*, 61, 1853–1868, doi:10.1002/lno.10338, 2016.

394 Kahru, M., Elmgren, R., and Savchuk, O. P.: Changing seasonality of the Baltic Sea, *Biogeosciences*, 13, 1009–1018, doi:10.5194/bg-13-
395 1009-2016, 2016.

396 Lau, K. and Weng, H.: Climate signal detection using wavelet transform: How to make a time series sing, *Bulletin of the American Meteoro-*
397 *logical Society*, 76, 2391–2402, doi:10.1175/1520-0477(1995)076<2391:csduwt>2.0.co;2, 1995.

398 Meier, H. E. M. and Kauker, F.: Modeling decadal variability of the Baltic Sea : 2 . Role of freshwater inflow and large-scale atmospheric
399 circulation for salinity, *Journal of Geophysical Research*, 108, 1–16, doi:10.1029/2003JC001799, 2003.

400 Meier, H. E. M., Döscher, R., and Faxén, T.: A multiprocessor coupled ice- ocean model for the Baltic Sea: application to the salt inflow.,
401 *Journal of geophysical research*, 108, doi:10.1029/2000JC000521, 2003.

402 Meier, H. E. M., Andersson, H. C., Arheimer, B., Blenckner, T., Chubarenko, B., Donnelly, C., Eilola, K., Gustafsson, B. G., Hansson, A.,
403 Havenhand, J., Höglund, A., Kuznetsov, I., MacKenzie, B. R., Müller-Karulis, B., Neumann, T., Niiranen, S., Piwowarczyk, J., Raudsepp,
404 U., Reckermann, M., Ruoho-Airola, T., Savchuk, O. P., Schimanke, S., Väli, G., Weslawski, J.-M., and Zorita, E.: Comparing
405 reconstructed past variations and future projections of the Baltic Sea ecosystem—first results from multi-model ensemble simulations,
406 *Environmental Research Letters*, 7, 034 005, doi:10.1088/1748-9326/7/3/034005, 2012.

407 Meier, H. E. M., Höglund, A., Eilola, K., and Almroth-Rosell, E.: Impact of accelerated future global mean sea level rise on hypoxia in the
408 Baltic Sea, *Climate Dynamics*, pp. 1–10, doi:10.1007/s00382-016-3333-y, 2017.

409 Meier, H. E. M., Väli, G., Naumann, M., Eilola, K., and Frauen, C.: Recently accelerated oxygen consumption rates amplify deoxygenation
410 in the Baltic Sea., *Journal of Geophysical Research*, in press.

411 Menden-Deuer, S. and Lessard, E. J.: Carbon to volume relationships for dinoflagellates, diatoms, and other protist plankton, *American*
412 *Society of Limnology and Oceanography*, 3, doi:10.4319/lo.2000.45.3.0569, 2000.

413 Parker, R. A.: Dynamic models for ammonium inhibition of nitrate uptake by phytoplankton, *Ecological Modelling*, 66, 113–120,
414 doi:10.1016/0304-3800(93)90042-Q, 1993.

415 Rakko, A. and Seppälä, J.: Effect of salinity on the growth rate and nutrient stoichiometry of two Baltic Sea filamentous cyanobacterial
416 species., *Estonian Journal of Ecology*, 63, 55–70, doi:10.3176/eco.2014.2.01, 2014.

417 Redfield, A. C.: The biological control of chemical factors in the environment, *American Scientist*, 46, 205–221, doi:10.5194/bg-11-1599-
418 2014, 1958.

419 Ruoho-Airola, T., Eilola, K., Savchuk, O. P., Parviainen, M., and Tarvainen, V.: Atmospheric nutrient input to the baltic sea from 1850 to
420 2006: A reconstruction from modeling results and historical data, *Ambio*, 41, 549–557, doi:10.1007/s13280-012-0319-9, 2012.

421 Savchuk, O. P.: Large-Scale Dynamics of Hypoxia in the Baltic Sea, in: Chemical structure of pelagic redox interfaces: Observation and
422 modeling, *Hdb Env Chem*, edited by Yakushev, E. V., pp. 137–160, Springer-Verlag, Berlin Heidelberg, doi:10.1007/698_2010_53, 2010.

423 Savchuk, O. P.: Large-Scale Nutrient Dynamics in the Baltic Sea, 1970–2016, *Frontiers in Marine Science*, 5, 95,
424 doi:10.3389/fmars.2018.00095, <https://www.frontiersin.org/article/10.3389/fmars.2018.00095>, 2018.

425 Savchuk, O. P., Wulff, F., Hille, S., Humborg, C., and Pollehne, F.: The Baltic Sea a century ago — a reconstruction from model simulations,
426 verified by observations, *Journal of Marine Systems*, 74, 485–494, doi:10.1016/j.jmarsys.2008.03.008, [http://linkinghub.elsevier.com/
427 retrieve/pii/S0924796308000572](http://linkinghub.elsevier.com/retrieve/pii/S0924796308000572), 2008.

428 Savchuk, O. P., Gustafsson, B. G., Rodríguez, M., Sokolov, A. V., and Wulff, F. V.: External nutrient loads to the Baltic Sea , 1970-2006,
429 2012.

430 Schernewski, G. and Neumann, T.: The trophic state of the Baltic Sea a century ago: a model simulation study, *Journal of marine systems*,
431 53, 109–124, doi:<https://doi.org/10.1016/j.jmarsys.2004.03.007>, 2004.

432 Schimanke, S. and Meier, H.: Decadal to centennial variability of salinity in the Baltic Sea, *Journal of Climate*, pp. JCLI–D–15–0443.1,
433 doi:10.1175/JCLI-D-15-0443.1, <http://journals.ametsoc.org/doi/10.1175/JCLI-D-15-0443.1>, 2016.

434 Stigebrandt, A. and Gustafsson, B. G.: Improvement of Baltic Proper Water Quality Using Large-scale Ecological Engineering., *AMBIO: A
435 Journal of the Human Environment*, 36, doi:10.1579/0044-7447(2007)36[280:IOBPWQ]2.0.CO;2, 2007.

436 Tamminen, T. and Andersen, T.: Seasonal phytoplankton nutrient limitation patterns as revealed by bioassays over Baltic Sea gradients of
437 salinity and eutrophication, *Marine Ecology Progress Series*, 340, 121–138, doi:10.3354/meps340121, 2007.

438 Torrence, C. and Compo, G. P.: A practical guide to wavelet analysis, *Bull. Amer. Meteor. Soc.*, pp. 61–78, 1998.

439 Vahtera, E., Conley, D. J., Gustafsson, B. G., Kuosa, H., Pitkanen, H., Savchuk, O. P., Tamminen, T., Viitasalo, M., Wasmund, N., and Wulff,
440 F.: Internal Ecosystem Feedbacks Enhance Nitrogen-fixing Cyanobacteria., *Ambio*, 36, 186–193, 2007.

441 Winder, M. and Cloern, J. E.: The annual cycles of phytoplankton biomass., *Philosophical transactions of the Royal Society of London.
442 Series B, Biological sciences*, 365, 3215–26, doi:10.1098/rstb.2010.0125, <http://rstb.royalsocietypublishing.org/content/365/1555/3215>,
443 2010.

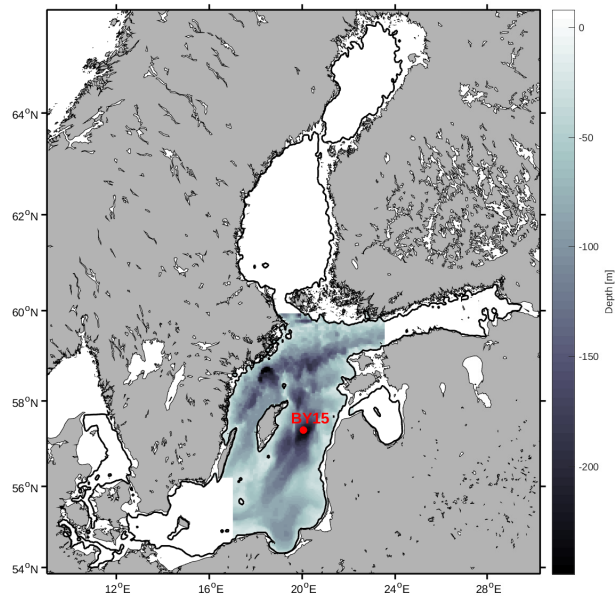


Figure 1. Study area. The grey scale represents depth in m. The red dot represents the monitoring station BY15

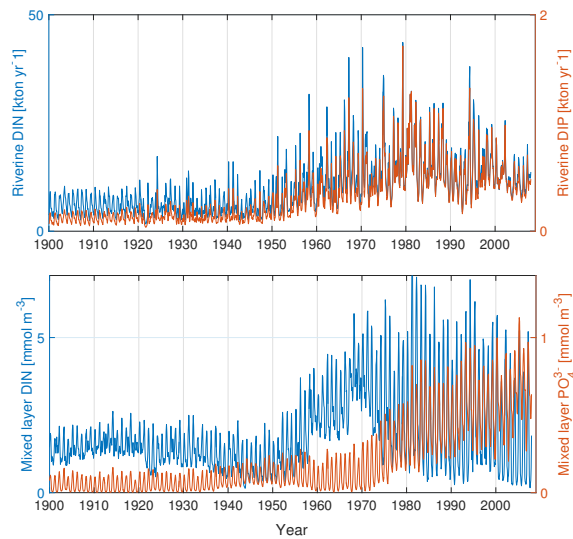


Figure 2. The top panel shows riverine DIN (blue) and DIP (red) loads to the Baltic proper as defined in Fig. 1. The bottom panel shows mixed layer DIN (blue) and mixed layer phosphate (red) averaged over the study area.

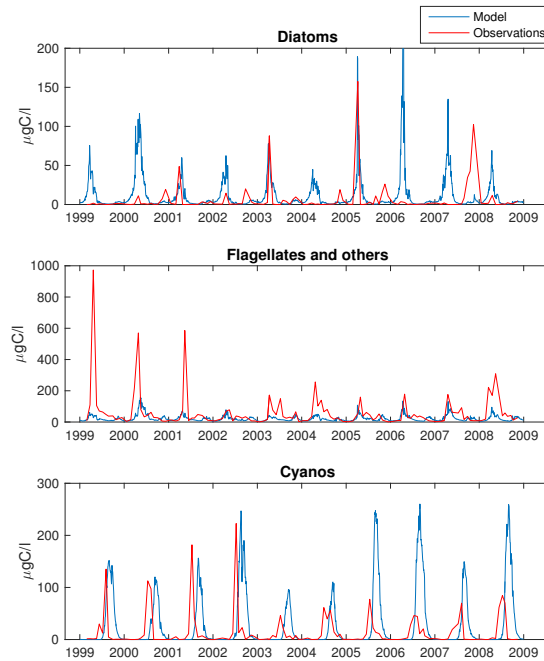


Figure 3. Simulated (blue) and observed (red) biomass of diatoms (top), flagellates and others (middle) and cyanobacteria (bottom) at BY15.

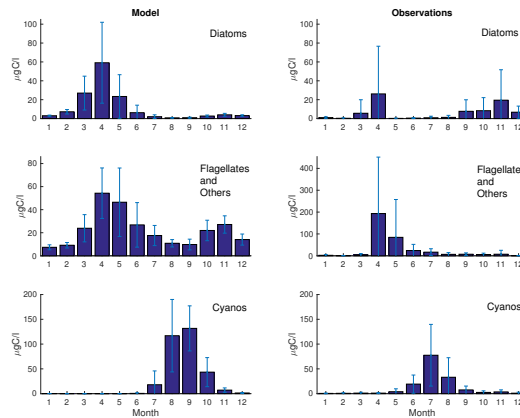


Figure 4. Monthly means of simulated (left) and observed (right) diatoms (top), flagellates and others (middle) and cyanobacteria (bottom) at BY15. Standard deviations are shown as errorbars.

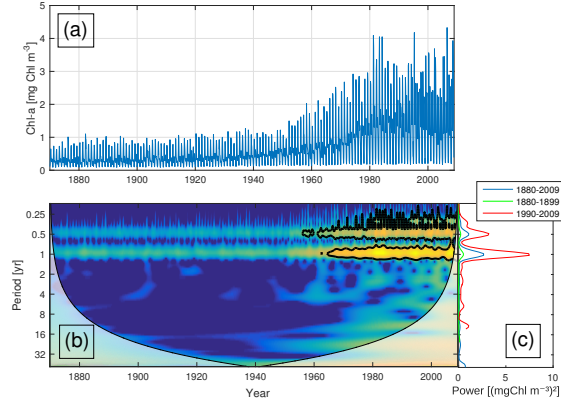


Figure 5. Time-series of phytoplankton biomass (a) together with the corresponding wavelet power spectrum (b) and global wavelet spectrum (c). More yellow means more power. The black curves in (b) represent the 95% confidence level relative to red noise. The white areas in (b) represent the cone of influence in which the results are impacted by edge-effects and are therefore not shown. The different lines in (c) represent the global spectrum 1880-2009 (blue), 1880-1899 (green), 1990-2009 (red).

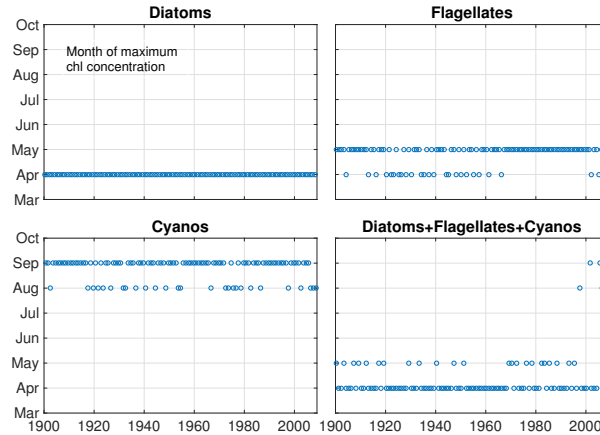


Figure 6. The month of maximum biomass of diatoms, flagellates and cyanobacteria as well as their sum.

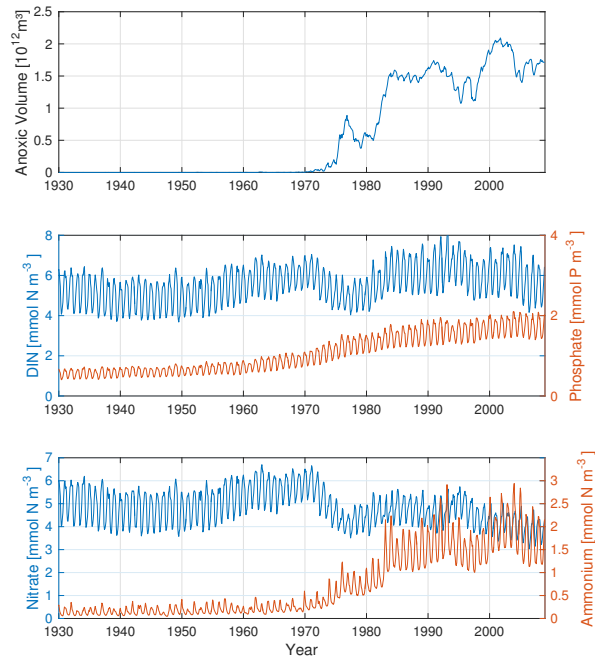


Figure 7. Time-series of anoxic volume (top), below mixed layer concentrations of DIN (nitrate + ammonium, blue) and phosphate (red) (middle) and nitrate (blue) and ammonium (red)(bottom) averaged over the Baltic proper.

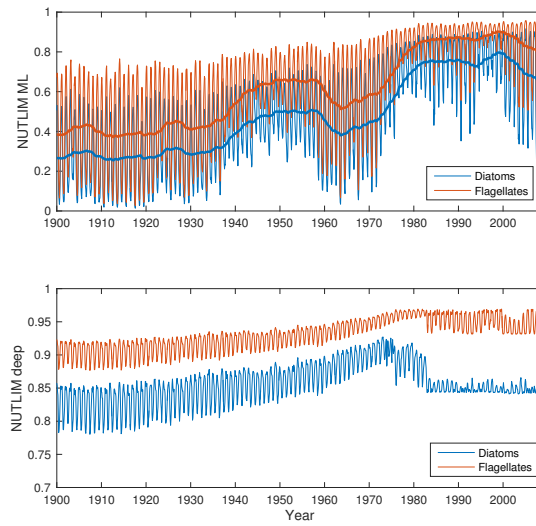


Figure 8. Time-series of nutrient limitation in the mixed layer (top) and below (bottom) for diatoms (blue) and flagellates (red). The thicker lines in the top panel show the 5-year moving average.

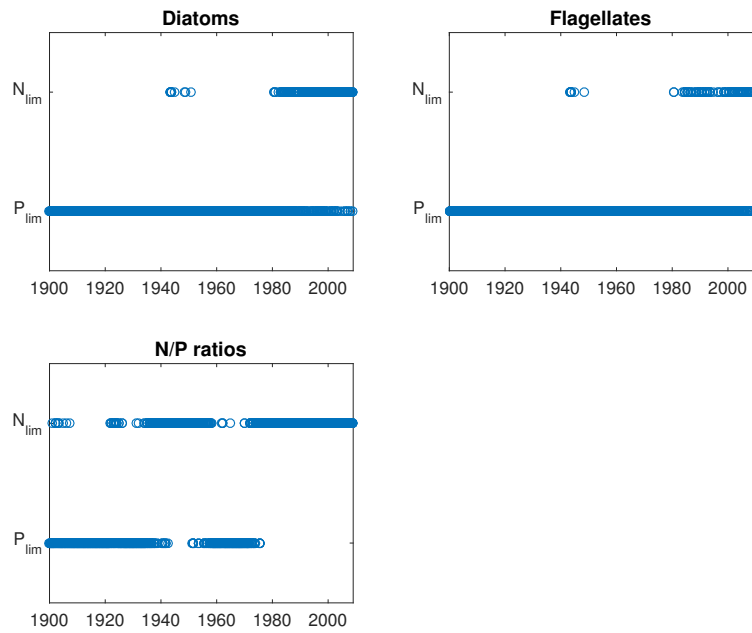


Figure 9. Mixed layer nitrogen or phosphate limitation as function of time for diatoms (upper left) and flagellates (upper right) as calculated through Eq. (2) where N limitation occurs when $N_{lim} < P_{lim}$. The bottom panel shows nutrient limitation as calculated through N/P ratios, where N limitation occurs when $N/P < 16$. Note that simultaneous N and P limitation is not possible although the size of the rings gives this appearance.

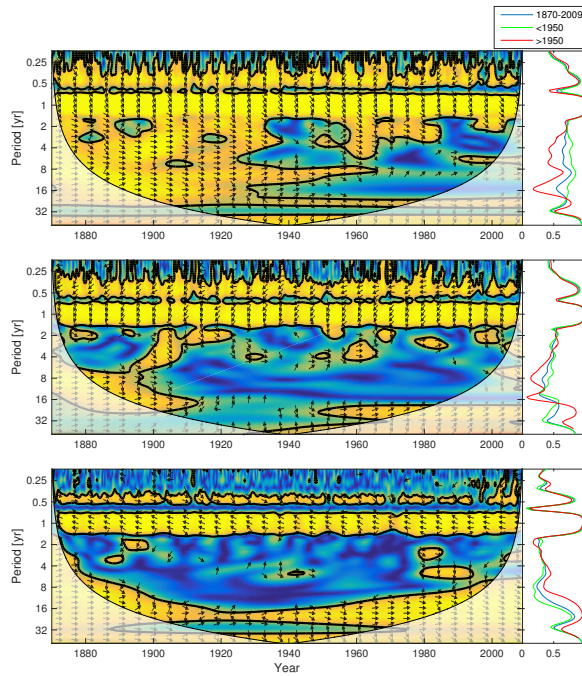


Figure 10. Wavelet coherence between mixed layer phosphate concentration and diatoms (top), flagellates (middle) and cyanobacteria (bottom). More yellow means more coherence. The arrows indicate the phase lag. When pointing to the right the two time-series are in phase and when pointing in the opposite direction anti-phase. The right panels show the coherence averaged over the whole period (blue) and before (green) and after (red) 1950.

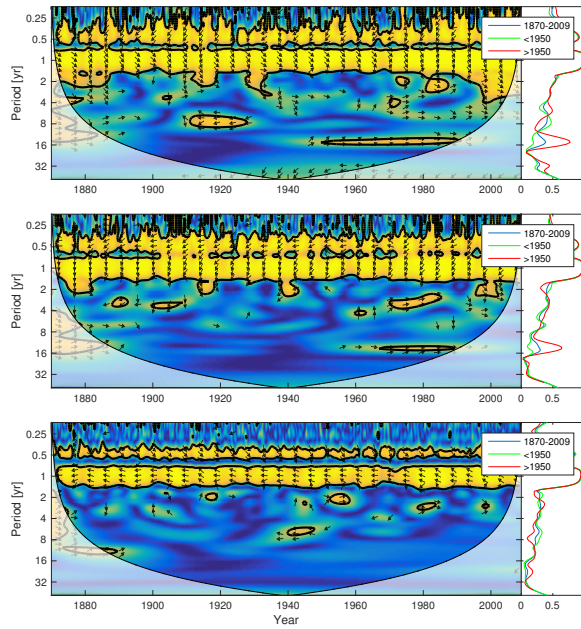


Figure 11. Wavelet coherence between mixed layer DIN concentration and diatoms (top), flagellates (middle) and cyanobacteria (bottom).

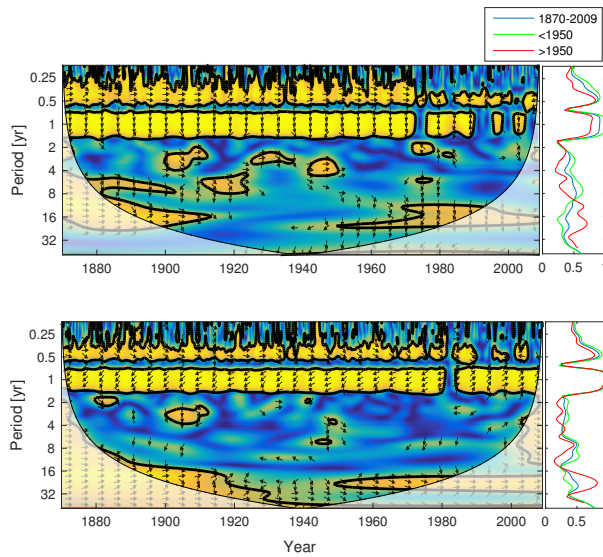


Figure 12. Wavelet coherence between deep water NUTLIM and diatoms (top), flagellates (middle)

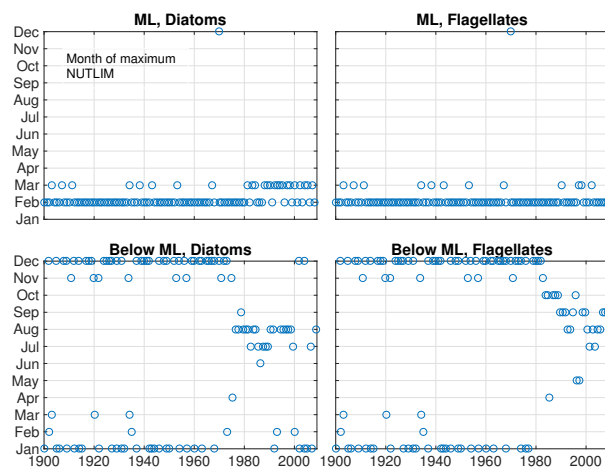


Figure 13. The month of maximum NUTLIM for diatoms (left) and flagellates (right) in the mixed layer (top) and below (bottom).

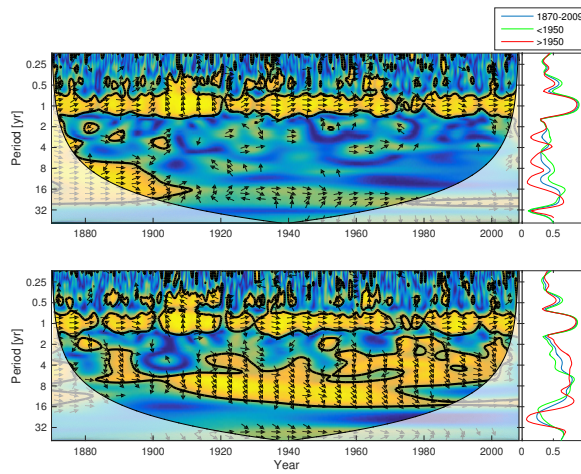


Figure 14. Wavelet coherence between riverine phosphate and mixed layer phosphate concentration (top) and riverine DIN and mixed layer DIN concentration (bottom). The arrows indicates the phase lag. When pointing to the right the two time-series are in phase and when pointing in the opposite direction anti-phase. The right panels show the averaged coherence for the whole period (blue) and before (green) and after (red) 1950.

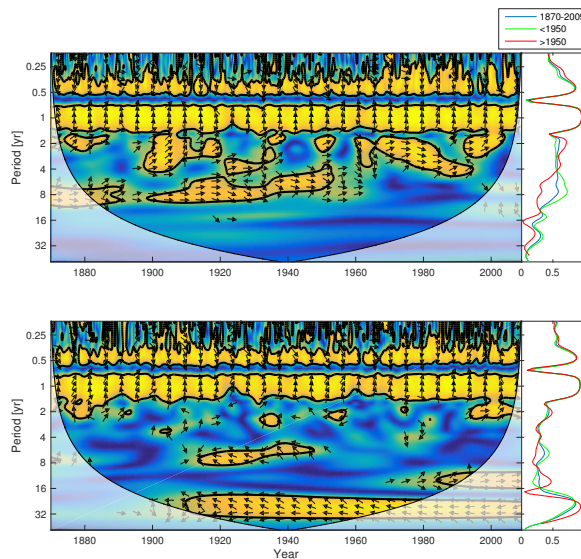


Figure 15. Wavelet coherence between mixed layer salinity and phosphate concentration (top) and mixed layer salinity and nitrate concentration (bottom). The right panels show the averaged coherence spectrum.

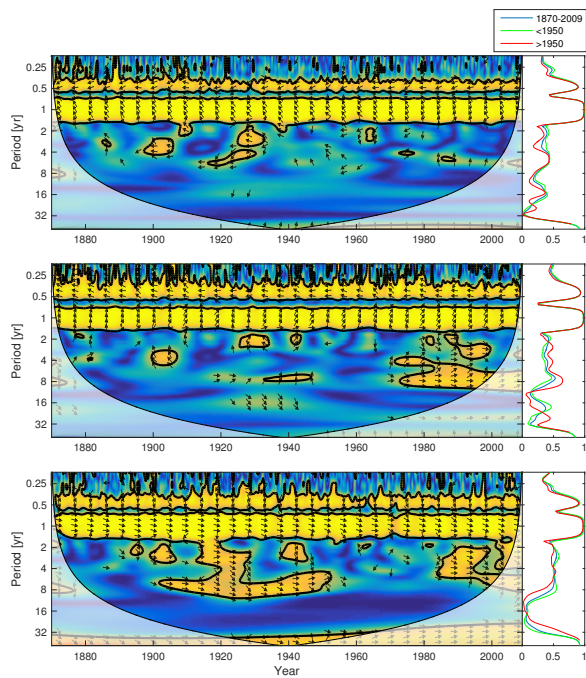


Figure 16. Wavelet coherence between mixed layer temperature and diatoms (top), flagellates (middle) and cyanobacteria (bottom).

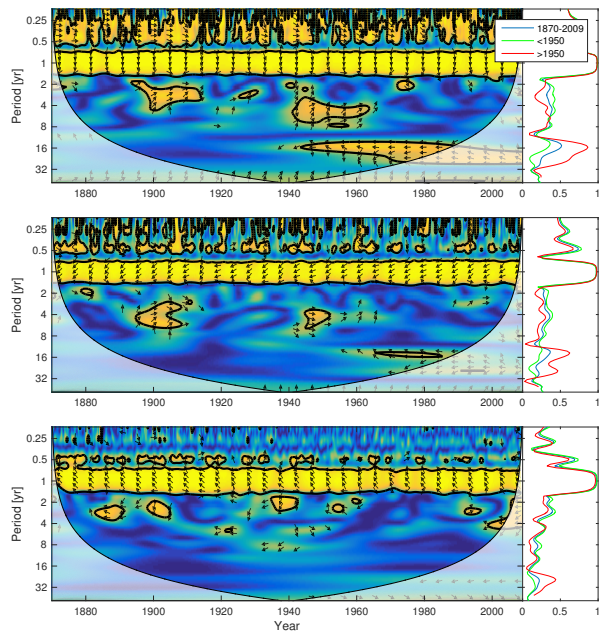


Figure 17. Wavelet coherence between mixed layer depth and diatoms (top), flagellates (middle) and cyanobacteria (bottom).